MEASUREMENT AND ANALYSIS OF THE $pd \to {}^3\mathrm{He}\eta$ REACTION BETWEEN 930 AND 1100 MeV*

J. Złomańczuk[a]

for the WASA-PROMICE Collaboration:

R. Bilger[b], W. Brodowski[b], H. Calén[c], H. Clement[b], C. Ekström[c]
G. Fäldt[a], K. Fransson[a], L. Gustafsson[a], B. Höistad[a], A. Johansson[a]
T. Johansson[a], K. Kilian[d], S. Kullander[a], A. Kupsc[c], G. Kurz[b]
P. Marciniewski[a], B. Morosov[e], A. Mörtsell[a], W. Oelert[d]
V. Renken[d], R.J.M.Y. Ruber[c], B. Shwartz[f], J. Stepaniak[g]
A. Sukhanov[e], P. Thörngren-Engblom[a], A. Turowiecki[h]
G.J. Wagner[b], Z. Wilhelmi[h], C. Wilkin[i] and J. Zabierowski[j]

[a]Department of Radiation Sciences, Uppsala University, 751-21 Uppsala, Sweden
[b]Physikalisches Institut, Tübingen University, 72076 Tübingen, Germany
[c]The Svedberg Laboratory, 751-21 Uppsala, Sweden
[d]IKP — Forschungszentrum Jülich GmbH, 52425 Jülich, Germany
[e]Joint Institute for Nuclear Research Dubna, 101 000 Moscow, Russia
[f]Budker Institute of Nuclear Physics, Novosibirsk 630 090, Russia
[g]Soltan Institute for Nuclear Studies, 00-681 Warsaw, Poland
[h]Institute of Experimental Physics, Warsaw University, 00-681 Warsaw, Poland
[i]Physics and Astronomy Dept., UCL, London WC1E 6BT, U.K.
[j]Soltan Institute for Nuclear Studies, 90-137 Łódz, Poland

(Received February 5, 2002)

Recent measurements of the $pd \to {}^3\mathrm{He}\,\eta$ reaction at four beam energies: 930, 965, 1037 and 1100 MeV have shown that the total cross section is nearly constant throughout the whole energy region, despite the CM angular distributions becoming more anisotropic with increasing energy. The data join smoothly onto the results of near-threshold measurements, which are dominated by the s-wave $\eta\,{}^3\mathrm{He}$ final state interaction. At all the energies the differential cross section is maximal for $\cos\theta_\eta \approx +0.5$. The data are used to develop a Monte Carlo description of the $pd \to {}^3\mathrm{He}\,\eta$ reaction based on a two-step model proposed by Kilian and Nann. With one free parameter the model qualitatively reproduces the excitation function in the energy range of this experiment but fails to reproduce the angular distributions.

PACS numbers: 25.40.–h, 25.10.+s, 25.40.Ve

* Presented at the VI TAPS Workshop, Krzyże, Poland, September 9–13, 2001.

1. Introduction

The results of the measurements of the $pd \to {}^3\mathrm{He}\,\eta$ cross section near threshold [1, 2] were surprising in that they showed an amplitude which decreased rapidly over an energy range of only a few MeV. Despite the dramatic fall, the Center-of-Momentum (CM) differential cross section remained rather isotropic. These features indicate a large $\eta\,{}^3\mathrm{He}$ s-wave scattering length, which might be associated with an $\eta\,{}^3\mathrm{He}$ quasi-bound state [3].

The striking features of the $pd \to {}^3\mathrm{He}\,\eta$ reaction initiated a lot of theoretical activity but the satisfactory understanding has not been reached yet. In 1988, Laget and Lecolley presented a microscopic calculation in which they used an elementary $\pi N \to \eta N$ amplitude, parameterized in terms of several N^* resonances [4]. In the calculation they included three-body mechanisms allowing the large momentum transfer, needed to produce η, to be shared between all three nucleons. This feature turned out to be very important since the two-body mechanisms were shown to underestimate the cross section by almost two orders of magnitude. The model was able to reproduce the high energy part (above $\sim$1400 MeV) of the experimental excitation function for $\theta_\eta = 180^\circ$. However, the low energy part was missed by more than an order of magnitude.

Kilian and Nann [5] have noticed that the η production cross section might be enhanced if the reaction proceeds as a sequence of two steps, $pp \to d\pi^+$ and $\pi^+ n \to p\eta$, followed by fusion of p and d into ${}^3\mathrm{He}$. They have also argued that close to threshold the intermediate particles: n, d and π^+ are nearly on the mass shell and, in addition, the deuteron produced in the first step and the proton produced in the second step have similar velocities so they can easily fuse into ${}^3\mathrm{He}$. The last feature is usually referred to as "magic kinematics". In the Kilian and Nann approach both steps are simulated with a Monte Carlo (MC) program using particles obtained in the first step as input for the second step.

A quantum-mechanical implementation of these ideas predicts a cross section which is only about a factor of two lower than the experimental data [6].

The cross section of the reaction was recently been measured at a beam energy of 980 MeV [7] and found to be much larger than that observed near threshold. Taken together with the available higher energy data, this led the authors to suggest that the excitation function of the $pd \to {}^3\mathrm{He}\,\eta$ reaction might be described in a model that only included the $S_{11}(1535)$ baryon resonance and phase space. In support of this, they argued that the effects of the $\eta\,{}^3\mathrm{He}$ final state interaction were restricted to the near-threshold region. The authors also suggested that the classical two-step model failed to reproduce their experimental data.

The much higher statistics measurements of the $pd \to {}^3\mathrm{He}\,\eta$ reaction carried out at the CELSIUS storage ring in Uppsala at four beam energies: 930, 965, 1037 and 1100 MeV, have shown that the CM η angular distributions are becoming highly anisotropic with increasing energy [8]. However, the distributions are not forward peaked as in the case of the $pd \to {}^3\mathrm{He}\,\pi^0$ reaction [9]. Since the $pd \to {}^3\mathrm{He}\,\pi^0$ reaction is well described in terms of empirical $pn \to d\pi^0$ amplitudes [10], the difference in the π^0 and η angular distributions may be taken as another indication that two-body mechanisms are suppressed in the $pd \to {}^3\mathrm{He}\,\eta$ reaction.

In this contribution we shall briefly review the results of the Uppsala experiment and present a two-step MC model developed to describe the experimental data.

2. Experiment

The Uppsala experiment was performed at the CELSIUS storage ring of The Svedberg Laboratory, using the WASA/PROMICE experimental set-up. The detector system, described in detail in Ref. [11], is shown schematically in Fig. 1. The Forward Detector (FD), which comprises four sets of plastic scintillation detectors and a tracker, provides reliable detection from 4.5° to 20°. The first set of scintillators after the forward exit window of the scattering chamber, labeled FWC, consists of four 3 mm thick segments and is used in the trigger to reduce background from interactions of the beam halo with the forward part of the beam pipe. The next set (FTH) comprises three 5 mm thick layers. The first two layers are each divided into 24 spiral segments, whereas the third is made of 48 sector-like segments. The third set (FRH) contains four 11 cm thick layers, which are divided into 24 sectors and placed so that one FRH sector overlaps with two sectors of the third plane of the FTH. The FRH is followed by a veto hodoscope (FVH) containing 12 horizontal bars. In order to increase the amount of light collected, the FVH modules are read out by two photomultiplier (PM) tubes placed at both ends.

The Central Detector (CD) includes two arrays of CsI crystals designed to measure both charged particles and photons emitted with angles between 30° to 90°. These arrays are preceded by thin plastic scintillator detectors, used as veto counters in the case of photon detection and as ΔE counters for charged particles.

Since a correct energy measurement is crucial in this experiment, a special calibration procedure was developed in order to determine the response of the detector modules with sufficient accuracy. The method, involving measuring protons elastically scattered by a proton target in an energy range from 48 to 300 MeV, is described in Ref. [12]. It is also necessary to have

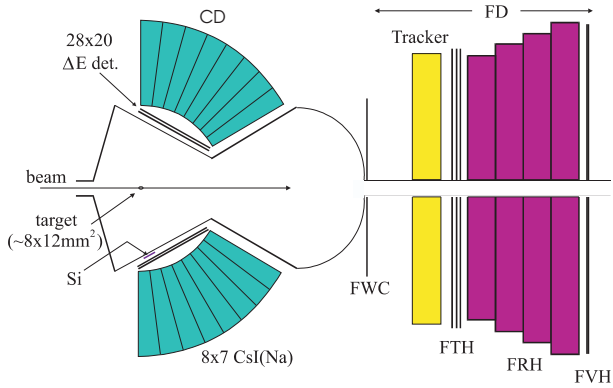

Fig. 1. Schematic representation of the PROMICE-WASA experiment.

good control of the gain stability to obtain a good energy resolution. For this purpose pulses from a light source were distributed to all detectors using optical fibers [13]. The stability of the light source was in turn checked with *pd* elastic scattering measured simultaneously with the ^{3}He production.

With various adjustments, described in detail in Ref. [8], an excellent missing mass resolution was achieved over the totality of the data at the four energies, as demonstrated in Fig. 2. The prominent η peak has a FWHM that changes with beam energy, from 3.4 MeV/c^2 at 930 MeV to 8.4 MeV/c^2 at 1100 MeV. Such narrow widths show not only good ^{3}He energy determination but also prove that any gain drift of the measuring electronics was properly corrected for. It is also worth noting that at all energies the background to the left and right of the peak can be joined smoothly.

In order to obtain distributions in the η CM angle with respect to the proton beam direction, θ_η, the whole range of $\cos\theta_\eta$ was divided into 20 bins and a missing mass distribution constructed for each of them. For the low-statistics samples, where both the ^{3}He and photons were detected in coincidence, only 10 bins were used. The η content was determined by fitting a polynomial function to regions outside of the peak and subtracting the resulting background.

The angular distributions have to be corrected for detector acceptance and this was done using a systematic Monte Carlo simulation of the detector response based on the GEANT3 program [14].

The differential cross sections have been normalized to both proton-deuteron elastic scattering and quasi-elastic proton-proton scattering. These were measured in parallel to the $pd \to {}^3\mathrm{He}\,\eta$ reaction by using a high-resolution silicon detector, placed at $\sim 75^\circ$, in coincidence with the FD (see Fig. 1). The $pd \to pd$ data were compared to the *pd* elastic cross section,

$$\frac{\mathrm{d}\sigma}{\mathrm{d}t} = 394\exp(-29.72|t| + 30.93t^2)\ [\mathrm{mb}/(\mathrm{GeV}/c)^2], \qquad (1)$$

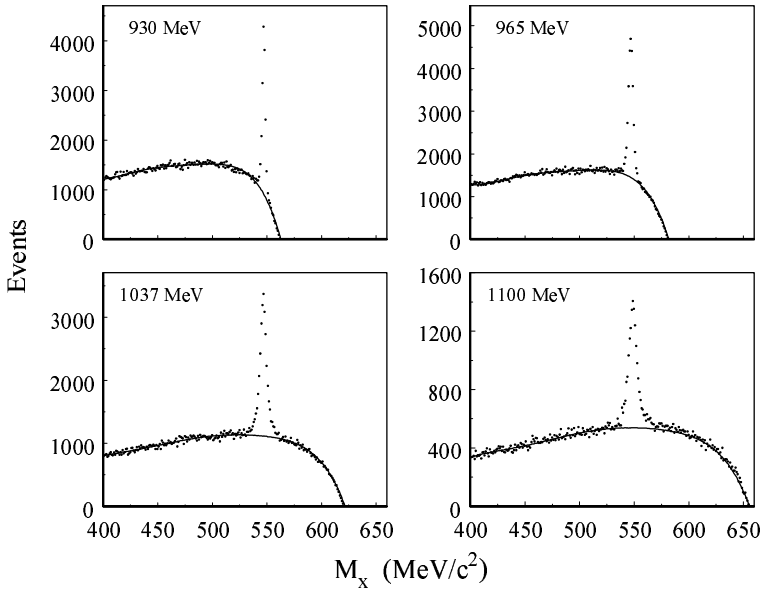

Fig. 2. Missing mass distributions of the $pd \to {}^3\mathrm{He}\,X$ reaction summed over angles and presented in 1 MeV/c^2 bins at our four energies. The curves represent polynomial fits to the regions outside of the η peak.

where t is the square of the four-momentum transfer. The parameters have been obtained by fitting existing elastic scattering data by Wilkenmann *et al.* [15] in an energy range close to the present experiment. The normalization of our quasi-elastic scattering data was adjusted to agree with the experimental results of Sai *et al.* [16]. The two methods gave luminosities which did not differ by more than a few percent.

The acceptance-corrected distributions in $\cos\theta_\eta$ are shown in Fig. 3. The full circles represent data where only the ^{3}He was detected, while the empty circles correspond to events where the ^{3}He and the two photons from the η decay were detected in coincidence. The good overlap between the two sets supports the correctness of the detector acceptance evaluation. In addition to the errors shown, there is an overall systematic uncertainty, which arises dominantly from the luminosity normalization (10%) but with minor contributions from the estimation of ^{3}He losses ($\leq 5\%$) and detector description ($\leq 5\%$). It is interesting to note that all the differential cross sections reported in this paper are maximal for $\cos\theta_\eta \approx 0.5$.

The points in the backward direction (full squares) have been taken from an interpolation of the systematic measurement of the excitation function at SPESIV at this angle [17]. The solid lines represent phenomenological fits

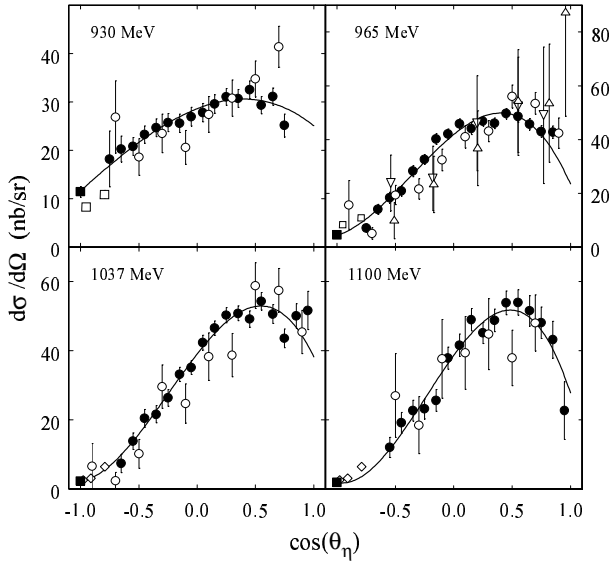

Fig. 3. Acceptance-corrected distributions in $\cos\theta_\eta$ obtained at our four beam energies. The full and empty circles represent data taken with only ^{3}He detected and with ^{3}He and two photons detected, respectively. The points in the backward direction (full squares) come from an interpolation of the Saclay SPESIV results [17]. The solid lines represent third order polynomial fits in $\cos\theta_\eta$. The open squares shown on the 930 and 965 MeV graphs and the open diamonds on the 1037 and 1100 graphs were taken from the SPESIV results at 950 and 1050 MeV, respectively [17]. The triangles on the 965 MeV graph are the GEM points [7] scaled by an empirical factor of 0.71.

to the experimental data with a third-order polynomial

$$\frac{d\sigma}{d\Omega_\eta} = a(1 + b\cos\theta_\eta + c\cos^2\theta_\eta + d\cos^3\theta_\eta)\,. \tag{2}$$

The values of χ^2 are very similar whether or not the backward SPESIV values are included in the fit, showing that our results are consistent with theirs. In order to constrain the fit better in the large angle region, the curves shown in Fig. 3 and the parameters listed in Table I, correspond to including the Saclay 180° results in the minimization. The errors on the parameters are purely statistical. The SPESIV group [17] also took data at a few angles close to 180°, although not at quite the same energies as ours. These points have been added to the most appropriate graphs. Also shown are data taken by the GEM collaboration at 980 MeV [7]. To compare the *shape* of their angular distribution with our results, these points have

been reduced by an empirical overall factor of 0.71. Even considering one high point at small angles, the differential distribution scaled in this way is compatible with our 965 MeV data.

TABLE I

Parameters obtained by fitting the η angular distributions with the formula of Eq. (2).

T_p (MeV)	a (nb/sr)	b	c	d	χ^2
930	28.6 ± 0.7	0.33 ± 0.07	-0.36 ± 0.11	-0.10 ± 0.15	0.35
965	41.9 ± 0.7	0.81 ± 0.05	-0.64 ± 0.07	-0.56 ± 0.09	1.27
1037	39.1 ± 0.8	1.10 ± 0.06	-0.48 ± 0.07	-0.65 ± 0.10	0.75
1100	38.6 ± 1.1	1.20 ± 0.09	-0.61 ± 0.09	-0.87 ± 0.14	0.85

The fits to the angular distributions presented in Fig. 4 have been used to obtain the total cross sections, $\sigma_{\rm tot}$, given in Table II with their statistical errors.

TABLE II

Total $pd \to {}^3\mathrm{He}\eta$ cross sections obtained in this work. The errors quoted are purely statistical.

T_p (MeV)	$\sigma_{\rm tot}$ (nb)
930	316 ± 16
965	413 ± 15
1037	412 ± 16
1100	386 ± 20

The comparison between the total cross sections measured here and those obtained in previous works is shown in Fig. 4. To display fully the very accurate experiments carried out close to threshold, it is useful to eliminate the phase space factor from the data by defining an average amplitude squared:

$$|f|^2 = \frac{p_p}{p_\eta} \frac{\sigma_{\rm tot}}{4\pi}, \tag{3}$$

where p_p and p_η are the CM momenta of the initial proton and final η. The steep fall in the amplitude over the first few MeV in excess energy is the sign of a very large $\eta\,{}^3$He scattering length, which might be associated

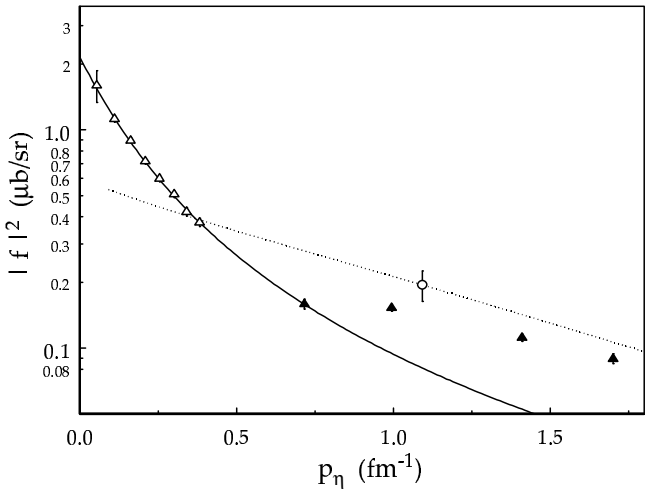

Fig. 4. Average amplitude squared of the $pd \to {}^3\mathrm{He}\,\eta$ reaction as a function of the CM η momentum. Empty and full triangles represent the SPESII results [2] and those of this work, respectively. The GEM point [7] is shown as an open circle. The solid curve, taken from Ref. [18], follows from a combined s-wave optical model fit to near-threshold $pd \to {}^3\mathrm{He}\,\eta$ and $\vec{d}d \to {}^4\mathrm{He}\,\eta$ data. The deviations of our points from the fit leave space for p and higher wave contributions. The resonance parameterization of Ref. [7] (dotted curve) does not describe well the near-threshold data [2] nor the results of this work.

with a quasi-bound η-nuclear state [3]. A combined optical model fit was made in Ref. [18] to the near-threshold $pd \to {}^3\mathrm{He}\,\eta$ and $\vec{d}d \to {}^4\mathrm{He}\,\eta$ data, assuming that the energy dependence is the result of an s-wave final state interaction. This prediction, which has here merely been extended in p_η, is meant to describe final s-waves in the $\eta\,{}^3\mathrm{He}$ system. The curve passes close to our 930 MeV point but diverges further from the higher ones. This is as expected, since the anisotropy of our angular distributions shown in Fig. 3 means that there are significant contributions from higher partial waves in addition to the s-wave.

3. Two-step model of the $pd \to {}^3\mathrm{He}\,\eta$ reaction

In the two-step model of Kilian and Nann [5], the $pd \to {}^3\mathrm{He}\,\eta$ reaction is assumed to proceed as a sequence of two processes, $pp \to d\pi^+$ and $\pi^+ n \to p\eta$, followed by fusion of the d from the first step and the p from the second step to form the ^{3}He. In addition, the particles produced in the first step are assumed to be on or close to their mass shells.

In this work we require the proton from the second step (see the diagram of Fig. 5) to be off-shell since it is not possible to form a ^{3}He nucleus from an on-shell proton and deuteron. The fusion is simulated using the spectator model with the deuteron being the spectator. This is easier to see if the graph of Fig. 5 is looked at from right to left: the ^{3}He splits into on-shell d' and off-shell p^*. The spectator model is based on two assumptions [21]:

- the spectator particle (d') influences the interaction only in terms of the associated Fermi motion,
- the matrix element for the quasi-free reaction on a bound target particle (p^*) is identical to that for the free reaction at the same energy.

We thus assume, that the p^* interacts with the η in the same way as an on-shell proton.

The spectator model is also used in the simulation of the $pp \to d\pi^+$ reaction. In this case the neutron from the initial deuteron is on-shell and acts as a spectator. Consequently, just as in the Kilian and Nann model, the three particles produced in the first step, *i.e.* d, π^+ and the spectator neutron are on the mass shell. In the second step the $\pi^+ n$ interaction leads to formation of one of the N^* resonances, which then decays into an on-shell η and off-shell proton p^* in such a way that p^* and d' can fuse into ^{3}He.

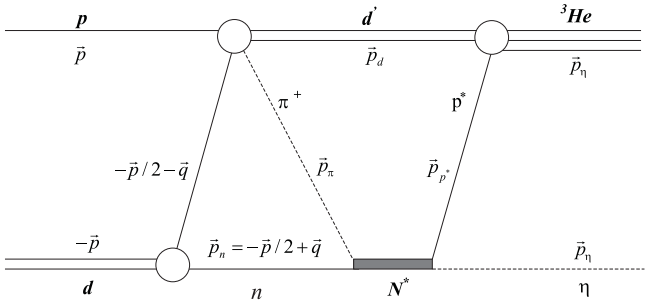

Fig. 5. Schematic representation of the two-step mechanism of the $pd \to {}^3\mathrm{He}\,\eta$ reaction.

The resulting probability of the $pd \to {}^3\mathrm{He}\,\eta$ reaction is then taken to be equal to

$$w_f = |\Psi_{^3\mathrm{He}}(q')|^2 \frac{p_\eta}{p_p} \frac{1}{d^2} d\sigma(\pi^+ n \to p\eta)/d\Omega \; d\sigma(pp \to d\pi^+)/d\Omega \; q^2 |\Psi_d(q)|^2 \,. \tag{4}$$

$\Psi_d(q)$ represents the S-state deuteron wave function, here taken from the Paris model [22]. The parameter q is the nucleon momentum in the deuteron rest frame. The ^{3}He wave function, $\Psi_{^3\mathrm{He}}(q')$, has been taken from Ref. [24]. The parameter q' is equal to the d' momentum in the ^{3}He rest frame. The differential cross section $d\sigma(pp \to d\pi^+)/d\Omega$ is obtained by linear interpolation over a two-dimensional matrix of data on the $pp \to d\pi^+$ reaction extracted with the SAID program [23]. The quantity d represents the distance between the pion production vertex and the spectator neutron and it has been taken to be equal to $\hbar/q$. Note that, due to the large momentum transfer, the pion production region is small compared to the internucleon distance in the deuteron ($\approx \hbar/q$ from the uncertainty principle).

The $\pi^+ n \to \eta p$ cross section is poorly known so a parameterization of the results of work of Batinić *et al.* [25] on the multiresonance coupled channel model of the $\pi^- p \to \eta n$ reaction has been used. For energies, W, below the $p + \eta$ mass, $d\sigma(\pi^- p \to \eta n)/d\Omega$ has been replaced with $|M(W)|^2 |\vec{p}_\eta|/|\vec{p}_\pi|$, where $|M(W)|^2$ was approximated by the Breit–Wigner form

$$|M(W)|^2 = \frac{A W_R^2 \Gamma_R^2}{\left(W_R^2 - W^2\right)^2 + W_R^2 \Gamma(W)^2}\,, \tag{5}$$

with W_R=1.544 GeV and Γ_R=0.203 GeV, as taken from the work of Krusche [26]. The S_{11} resonance width $\Gamma(W)$ is strongly energy dependent because the resonance is located very close to the η-production threshold. The parameter A=0.314 mb has been adjusted to provide a continuous transition between the two regions (see Fig. 6).

The weight (4) leads to the excitation function shown in Fig. 7. In order to fit the Uppsala experimental points, the MC distribution had to be divided by a factor of 3.6, though this is not unexpected given the crudeness of the estimate for d. As one can see, the MC curve roughly follows the Uppsala data. However, the amplitude squared decreases for small energies and at threshold is about a factor of three lower than at 965 MeV, in disagreement with the experiment. It should be noted that this result is in agreement with the quantum-mechanical treatment of Fäldt and Wilkin [6], where it has been shown that the rapid increase of the amplitude squared near threshold is to be attributed to the η^3He final state interaction. Similar results have also been obtained by Khemchandani *et al.* [27]. They have shown that near threshold the two-step model gives a matrix element squared which is constant and the experimentally observed increase is again attributed to the η^3He final state interaction.

While the model describes qualitatively the shape of the excitation function in the Uppsala energy range, it fails completely to reproduce the angular distributions. This is shown in Fig. 8, where the experimental angular distributions are compared to the simulated ones. As one can see the simulation

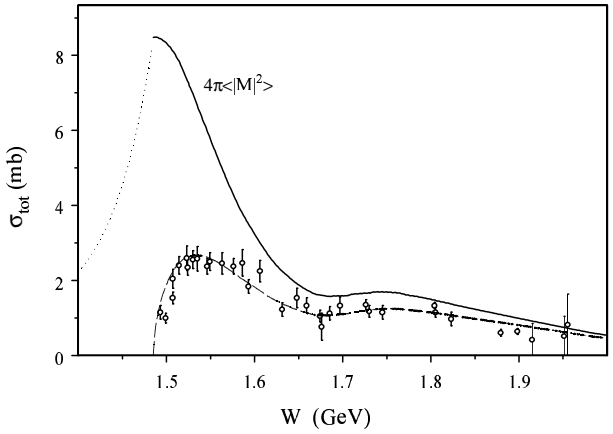

Fig. 6. Experimental excitation function of the $\pi^- p \to n\eta$ reaction (circles) taken from Ref. [28] compared to the parameterization of the results of Ref. [25] (dashed line). Solid line is the total cross section with the phase space factor removed ($\sigma_{\rm tot} p_\pi / p_\eta$) and the dotted line represents its extension to the energies below the $n + \eta$ mass, as calculated using Eq. (5). This shows a typical cusp structure of a type which is well known at the η threshold.

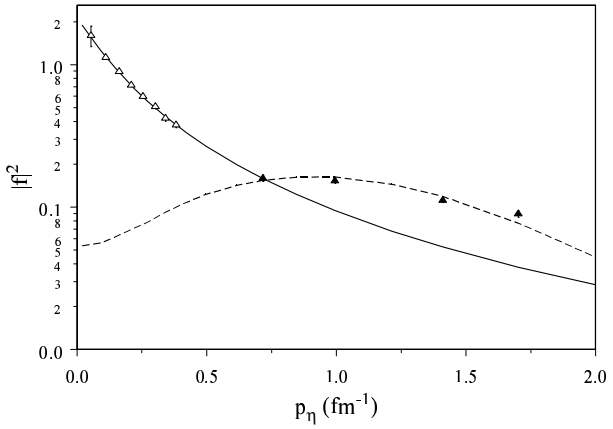

Fig. 7. Excitation function for the $pd \to {}^3$He η reaction obtained in the MC simulation with the weight given by the expression (4) (dashed curve). The experimental points and solid curve are the same as in Fig. 4.

is not even able to reproduce the sign of the slope. It is worth noting that a similar result at a lower energy has been obtained in Ref. [27]; the calculated η-production is larger in the backward hemisphere.

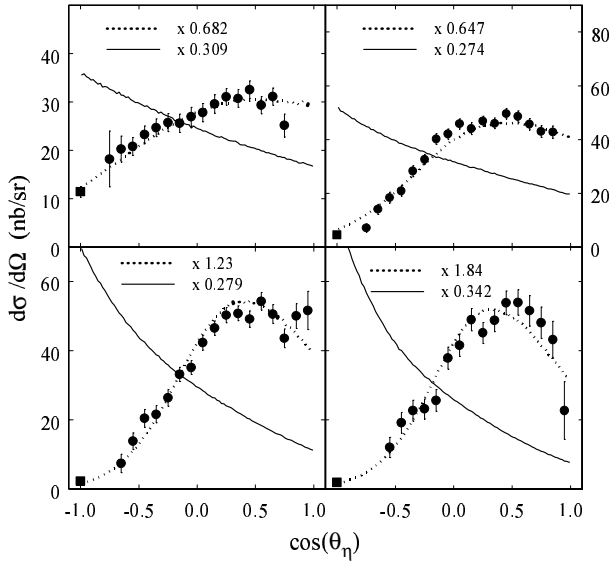

Fig. 8. Angular distributions obtained in the MC simulation of the $pd \to {}^3\mathrm{He}\,\eta$ reaction compared to the experimental data. Solid lines represent unconstrained distributions. The distributions presented with dotted lines have been obtained for the pion-neutron relative cut-off angle changing from about 100° at 930 MeV to ∼70° at 1100 MeV. At each energy, both constrained and unconstrained distributions, were normalized to the total cross section corresponding to that energy. The resulting normalization factors are indicated in the panels. The experimental data are the same as in Fig. 3.

The fact that the two-step model gives nearly the right total cross section while getting the angular distribution wrong suggests that it is missing something. While the basic concept that the reaction proceeds as a sequence of two processes seems to be well established, the correctness of the assumption on the reaction of the second step, *i.e.* $\pi^+ n \to p\eta$, proceeding as on a free target is not so obvious. To make it more clear a hypothetical arrangement of nucleons before and after the pp collision is presented in Fig. 9.

As shown in the figure, the spectator neutron is practically inside of the newly produced deuteron, d', so the chance that they interact is high. In addition, the large momentum transfer needed to produce a π^+ ($\sim \sqrt{m_\pi m_p}$= 0.36 GeV/c at threshold) requires the initial protons to approach each other closely. As a consequence, the distance between nucleons in the newly formed d' is much shorter than the one corresponding to the average in a physical deuteron. But the d' must eventually assume the normal deuteron state so the nucleons have to move outward, which leads to a further increase

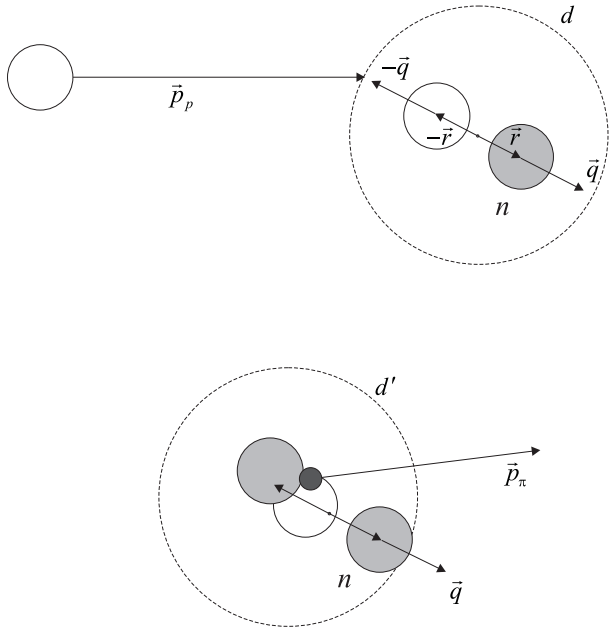

Fig. 9. Schematic representation of the quasi-free $pp \to d\pi^+$ reaction on a deuteron target. The upper part represents the incoming proton and the initial deuteron (d) just before the collision. The neutron (n) in the initial deuteron is a spectator. The lower part shows positions of particles just after the collision with the spectator neutron within the newly created deuteron (d').

of the interaction rate with the spectator neutron. The chances for the spectator neutron not to interact with the d' increase when the nucleons in the initial deuteron move outward. This is a consequence of the fact that in such a case the spectator is escaping from the volume occupied by the d'. Combined with the observation, that π^+ is produced in close vicinity of the participating proton in the initial deuteron ($\Delta r \approx 0.55$ fm), this imposes a correlation between the directions of $\vec{p}_\pi$ and $\vec{q}$; the probability for the $\pi^+ n \to \eta p$ reaction to take place is enhanced when the π^+ an n are moving in similar directions.

In order to test if such a correlation exists the η angular distributions have been obtained with various cuts imposed on the relative $\pi^+ - n$ angle, $\theta_{\pi n}$. A nearly perfect match between the experimental and simulated distributions for events with $\theta_{\pi n}$ not exceeding about 100° at 930 MeV and ∼70° at 1100 MeV indicates (dotted line in Fig. 8), that the correlation really exists. This in turn suggests that losses of the spectator neutrons due to interactions with deuterons may be important.

4. Conclusions

We have measured the differential cross section of the $pd \to {}^3\mathrm{He}\,\eta$ reaction in a transition region where higher partial waves are starting to emerge. The distributions become strongly anisotropic with increasing energy, although not peaking in the forward direction. Comparison with the $pd \to {}^3\mathrm{He}\pi^0$, where the π^0 angular distributions strongly peak in the forward direction [9], suggests that the two reactions are driven by different mechanisms.

The two-step MC model developed in this work describes the shape of the excitation function of the $pd \to {}^3\mathrm{He}\,\eta$ reaction in the energy range of our experiment but misses the absolute value by a factor of ~ 3.6. The experimentally observed enhancement of the cross section near threshold is not reproduced if the ${}^3\mathrm{He}\,\eta$ final state interaction is not included into the model.

The CM angular distributions of η predicted by the model are peaked in the backward direction so that they do not agree with the experiment. However, the shape of the angular distributions may be changed to match the experimental ones by imposing a condition on the relative pion-neutron angle. This observation suggests that $\pi^+ n \to p\eta$ reaction is affected by the presence of deuterons from the first step.

We are very grateful to the TSL/ISV personnel for their continued help during the course of this work. Financial support for this experiment and its analysis was provided by the Swedish Natural Science Research Council, the Swedish Royal Academy of Science, the Swedish Institute, Deutsche Forschung Gesellschaft (Mu 705/3 Graduiertenkolleg), the Polish State Committee for Scientific Research (KBN) no 621/E-78/SPUB-M, the Russian Academy of Science, the German Bundesministerium für Bildung und Forschung [06TU886 and DAAD], and the European Science Exchange Program.

REFERENCES

[1] J. Berger *et al.*, *Phys. Rev. Lett.* **61**, 919 (1988).
[2] B. Mayer *et al.*, *Phys. Rev.* **C53**, 2068 (1996).
[3] C. Wilkin, *Phys. Rev.* **C47**, R938 (1993).
[4] J.-M. Laget, J.-F. Lecolley, *Phys. Rev. Lett.* **61**, 2069 (1988).
[5] K. Kilian, H. Nann, *AIP Conf. Proc.* **221**, 185 (1990).
[6] G. Fäldt, C. Wilkin, *Nucl. Phys.* **A587**, 769 (1995).
[7] M. Betigeri *et al.*, *Phys. Lett.* **B472**, 267 (2000).

[8] R. Bilger *et al.*, accepted for publication in *Phys. Rev.* **C**.
[9] V.N. Nikulin *et al.*, *Phys. Rev.* **C54**, 1732 (1996).
[10] J.-F. Germond, C. Wilkin, *J. Phys. G* **16**, 381 (1990).
[11] H. Calén *et al.*, *Nucl. Instrum. Methods Phys. Res.* **A379**, 57 (1996).
[12] R. Bilger *et al., Nucl. Phys.* **A693**, 633 (2001).
[13] J. Zabierowski, *Nucl. Instrum. Methods Phys. Res.* **A338**, 577 (1994).
[14] CERN Program Library Long Write-up W5013, *GEANT — Detector Description and Simulation Tool.*
[15] E. Winkelmann *et al.*, *Phys. Rev.* **C21**, 2535 (1980).
[16] F. Sai *et al.*, *Phys. Rev. Lett.* **55**, 2668 (1985).
[17] P. Berthet *et al.*, *Nucl. Phys.* **A443**, 589 (1985).
[18] N. Willis *et al.*, *Phys. Lett.* **B406**, 143 (1997).
[19] CERN Program Library Short Write-up W505 (1993) *FOWL.*
[20] CERN Program Library Long Write-up W515 (1993) *GENBOD.*
[21] F. Duncan *et al.*, *Phys. Rev. Lett.* **80**, 4390 (1998).
[22] M. Lacombe *et al.*, *Phys. Rev.* **C21**, 861 (1980).
[23] R.A. Arndt, I.I. Strakowsky, R.L. Workman, *Phys. Rev.* **C50**, 2731 (1994).
[24] J-F. Germond, C. Wilkin, *J. Phys. G: Nucl. Phys.* **14**, 181 (1988).
[25] M. Batinić *et al. Phys. Rev.* **C51**, 2310 (1995).
[26] B. Krusche, *Acta Phys. Pol.* **B27**, 3147 (1996).
[27] K.P. Khemchandani, N.G. Kelkar, B.K. Jain, `nucl-th/0112065`.
[28] V. Flaminio *et al.*, CERN-HERA report 83-0, 1983.